Supporting information

Modulating the electrocatalytic activity of mononuclear nickel complexes toward water oxidation by tertiary amine group

Xiaoli Chen[a], Xuehong Liao[a], Chang Dai[a], Lihong Zhu[a], Li Hong[a], Xueli Yang[a], Zhijun Ruan[*a], Xiangming Liang[*b], Junqi Lin[*a]

[a] Hubei Key Laboratory of Processing and Application of Catalytic Materials, College of Chemistry and Chemical Engineering, Huanggang Normal University, Huanggang, 438000 China.

Email: ruanzhijun87@126.com, linjunqi@hgnu.edu.cn

[b] School of Basic Medical Sciences, Ningxia Medical University, Yinchuan, 750004, China.

Email: liangxm6@163.com

Electrochemical tests: The GC electrode was subsequently polished with 300 nm and 50 nm aluminum oxide slurry for at least 3 min, followed by sonication in ethanol and distilled water separately for about 15 s, and then rinsed with ultrapure water. An indium tin oxide (ITO) electrode (1 cm^2 immersed in electrolyte) was used as the working electrode for the controlled potential electrolysis experiment. Before usage, the ITO electrode was cleaned by sonication in acetone, ethanol, and ultrapure water for half an hour, separately. Differential pulse voltammetry (DPV) tests were obtained with the following parameters: amplitude. = 50 mV, step height = 4 mV, pulse width = 0.05 s, pulse period = 0.5 s and sampling width = 0.0167 s.

Table S1 Crystallographic data and processing parameters for complexes **1**–**2**

Complex parameters	Complex **1**	Complex **2**
Empirical formula	$C_{16}H_{27}Cl_2N_5NiO_{10}$	$C_{19}H_{28}N_6Cl_2NiO_8$
Formula weight	579.02	598.08

Temperature / K	292(2)	296(2)
Wavelength / Å	0.71073	0.71073
Crystal system	Monoclinic	Triclinic
Space group	$P2_1/n$	P-1
a / Å	8.5418(9)	9.414(3)
b / Å	10.8038(10)	11.334(3)
c / Å	26.763(3)	13.582(3)
α / deg	90	86.743(9)
β / deg	92.943	73.749(10)
γ / deg	90	66.423(9)
Volume / Å^3	2466.5(4)	1272.7(6)
Z	4	2
Calculated density / Mg m^3	1.554	1.561
Absorption coefficient / mm^{-1}	1.062	1.028
F(000)	1192	620
Crystal size / mm^3	0.300 × 0.280 × 0.250	0.320 × 0.180 × 0.150
θ range / deg	2.033 to 25.099	1.964 to 25.077
Index ranges	-10≤h≤10 -12≤h≤12 -31≤h≤31	-11≤h≤11 -13≤k≤13 -16≤l≤16
Reflections collected	94397	37608
Independent reflections	4383[*R*(int) = 0.0607]	4505 [*R*(int) = 0.0889]
Completeness to theta	99.9 % (25.099°)	99.6 % (25.077°)
Refinement method	Full-matrix least-squares on F^2	
Data / restraints / parameters	4383 / 0 / 312	4505 / 0 / 327
Goodness-of-fit on F^2	1.031	1.027
Final R indices [I>2sigma(I)]	R_1 = 0.0517, wR_2 = 0.1569	R_1 = 0.0602, wR_2 = 0.1664
R indices (all data)	R_1 = 0.0562, wR_2 = 0.1623	R_1 = 0.0791, wR_2 = 0.1850
Largest diff. peak and hole	0.681 and -0.517 e.Å^{-3}	0.598 and -0.563 e.Å^{-3}

$R_1 = \Sigma||F_o| - |F_c||/\Sigma|F_o|$, $wR_2 = [\Sigma(|F_o|^2 - |F_c|^2)^2/\Sigma(F_{o2})]^{1/2}$

Table S2 Crystallographic data and processing parameters for complexes **3** and **5**

Complex parameters	Complex **3**	Complex **5**
Empirical formula	$C_{19}H_{31}N_5Cl_2NiO_9$	$C_{17}H_{27}N_5Cl_2ZnO_9$

Formula weight	603.10	581.70
Temperature / K	296(2)	293(2)
Wavelength / Å	0.71073	0.71073
Crystal system	Monoclinic	Monoclinic
Space group	$P2_1/c$	$P2_1/c$
a / Å	9.0633(12)	8.739(7)
b / Å	32.964(5)	17.836(14)
c / Å	8.8182(13)	15.852(14)
α / deg	90	90
β / deg	104.961(5)	100.78
γ / deg	90	90
Volume / Å^3	2545.3(6)	2427(3)
Z	4	4
Calculated density / Mg m^3	1.574	1.592
Absorption coefficient / mm^{-1}	1.030	1.289
F(000)	1256	1200
Crystal size / mm^3	0.320 × 0.280 × 0.250	0.270 × 0.260 × 0.250
θ range / deg	2.326 to 25.100	2.284 to 25.151
Index ranges	-10≤h≤10 -39≤k≤39 -10≤l≤10	-10<=h<=10 -21<=k<=21 -18<=l<=18
Reflections collected	77120	96721
Independent reflections	4521 [*R*(int) = 0.0476]	4280 [*R*(int) = 0.0648]
Completeness to theta	99.8 % (25.100°)	98.1 % (25.151°)
Refinement method	Full-matrix least-squares on F^2	
Data / restraints / parameters	4521 / 0 / 329	4280 / 0 / 309
Goodness-of-fit on F^2	1.065	1.013
Final R indices [I>2sigma(I)]	R_1 = 0.0498, wR_2 = 0.1471	R_1 = 0.0331, wR_2 = 0.0879
R indices (all data)	R_1 = 0.0535, wR_2 = 0.1504	R_1 = 0.0407, wR_2 = 0.0942
Largest diff. peak and hole	1.163 and -0.514 e.Å^{-3}	0.551 and -0.369 e.Å^{-3}

$R_1 = \Sigma||F_o| - |F_c||/\Sigma|F_o|$, $wR_2 = [\Sigma(|F_o|^2 - |F_c|^2)^2/\Sigma(F_{o2})]^{1/2}$

Table S3 Selected bond lengths (Å) and angles (deg) for complexes **1** and **2**

Complex	**1**	Complex	**2**
Bond length (Å)		Bond length (Å)	

Ni1–N1	2.070(3)	Ni1–N1	2.066(4)
Ni1–N2	2.115(3)	Ni1–N2	2.121(4)
Ni1–N3	2.111(3)	Ni1–N3	2.133(4)
Ni1–N4	2.063(3)	Ni1–N4	2.074(5)
Ni1–N5	2.075(3)	Ni1–N5	2.082(4)
Ni1–O1	2.136(3)	Ni1–N6	2.114(5)
Bond angles (deg)		Bond angles (deg)	
N1–Ni1–N2	80.19(12)	N1–Ni1–N2	80.90(16)
N1–Ni1–N3	94.92(12)	N1–Ni1–N3	96.67(17)
N1–Ni1–N4	176.89(12)	N1–Ni1–N4	175.3(2)
N1–Ni1–N5	101.96(11)	N1–Ni1–N5	100.26(16)
N1–Ni1–O1	90.29(12)	N1–Ni1–N6	92.09(16)
N2–Ni1–N3	83.99(12)	N2–Ni1–N3	83.57(18)
N2–Ni1–N4	97.56(13)	N2–Ni1–N4	94.4(2)
N2–Ni1–N5	96.49(11)	N2–Ni1–N5	95.05(16)
N2–Ni1–O1	170.19(13)	N2–Ni1–N6	172.79(17)
N3–Ni1–N4	82.68(13)	N3–Ni1–N4	83.45(19)
N3–Ni1–N5	162.96(13)	N3–Ni1–N5	162.59(18)
N3–Ni1–O1	94.55(12)	N3–Ni1–N6	95.64(18)
N4–Ni1–N5	80.37(12)	N4–Ni1–N5	79.35(19)
N4–Ni1–O1	91.87(14)	N4–Ni1–N6	92.6(3)
N5–Ni1–O1	87.75(11)	N5–Ni1–N6	87.84(16)

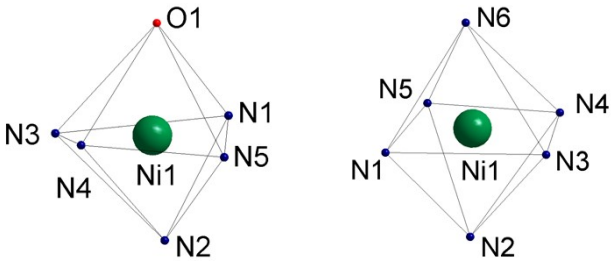

Fig. S1 The geometry configuration of complexes **1** and **2**.

Table S4 Selected bond lengths (Å) and angles (deg) for complexes **3** and **5**

Complex	**3**	Complex	**5**
Bond length (Å)		Bond length (Å)	

Ni1–N1	2.126(3)	Zn1–N1	2.135(3)
Ni1–N2	2.192(3)	Zn1–N2	2.167(3)
Ni1–N3	2.126(3)	Zn1–N3	2.219(3)
Ni1–N4	2.159(3)	Zn1–N4	2.134(3)
Ni1–N5	2.095(3)	Zn1–N5	2.119(3)
Ni1–O1	2.129(3)	Zn1–O1	2.247(3)
Bond angles (deg)		Bond angles (deg)	
N1–Ni1–N2	77.16(12)	N1–Zn1–N2	79.89(10)
N1–Ni1–N3	101.53(12)	N1–Zn1–N3	94.50(9)
N1–Ni1–N4	173.08(11)	N1–Zn1–N4	175.09(9)
N1–Ni1–N5	97.83(11)	N1–Zn1–N5	105.81(9)
N1–Ni1–O1	84.68(11)	N1–Zn1–O1	89.70(10)
N2–Ni1–N3	83.44(14)	N2–Zn1–N3	83.01(9)
N2–Ni1–N4	108.87(12)	N2–Zn1–N4	100.89(11)
N2–Ni1–N5	94.20(13)	N2–Zn1–N5	100.67(9)
N2–Ni1–O1	161.10(12)	N2–Zn1–O1	169.14(8)
N3–Ni1–N4	82.81(12)	N3–Zn1–N4	80.82(9)
N3–Ni1–N5	159.42(13)	N3–Zn1–N5	159.68(9)
N3–Ni1–O1	95.25(13)	N3–Zn1–O1	94.83(8)
N4–Ni1–N5	78.62(11)	N4–Zn1–N5	78.86(10)
N4–Ni1–O1	89.59(11)	N4–Zn1–O1	89.22(10)
N5–Ni1–O1	93.41(12)	N5–Zn1–O1	85.05(9)

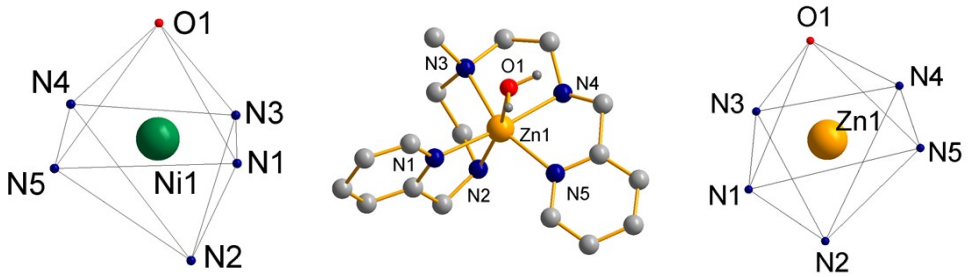

Fig. S2 The geometry configuration of complex **3** (left); ball-and-stick representation of X-ray crystal structures (middle) and geometry configuration of complex **5** (right).

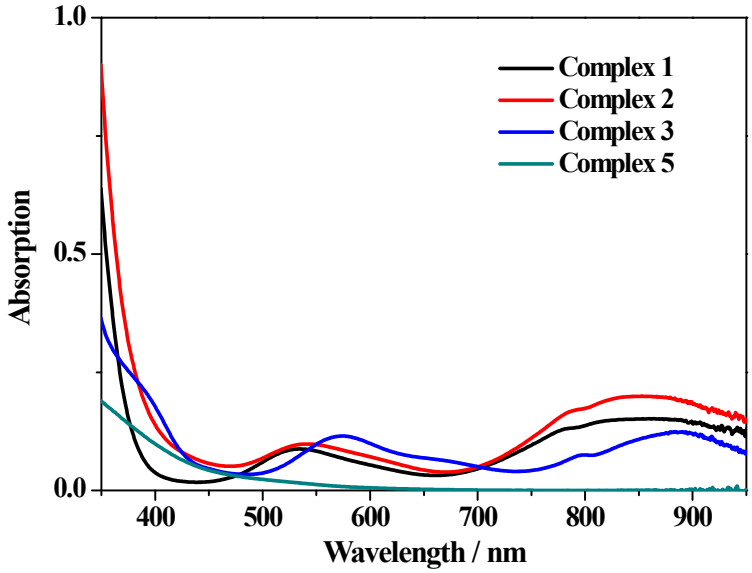

Fig. S3 UV-vis spectra of 10 mM complexes **1**–**3** and **5** in 0.1 M PBS at pH 9.0.

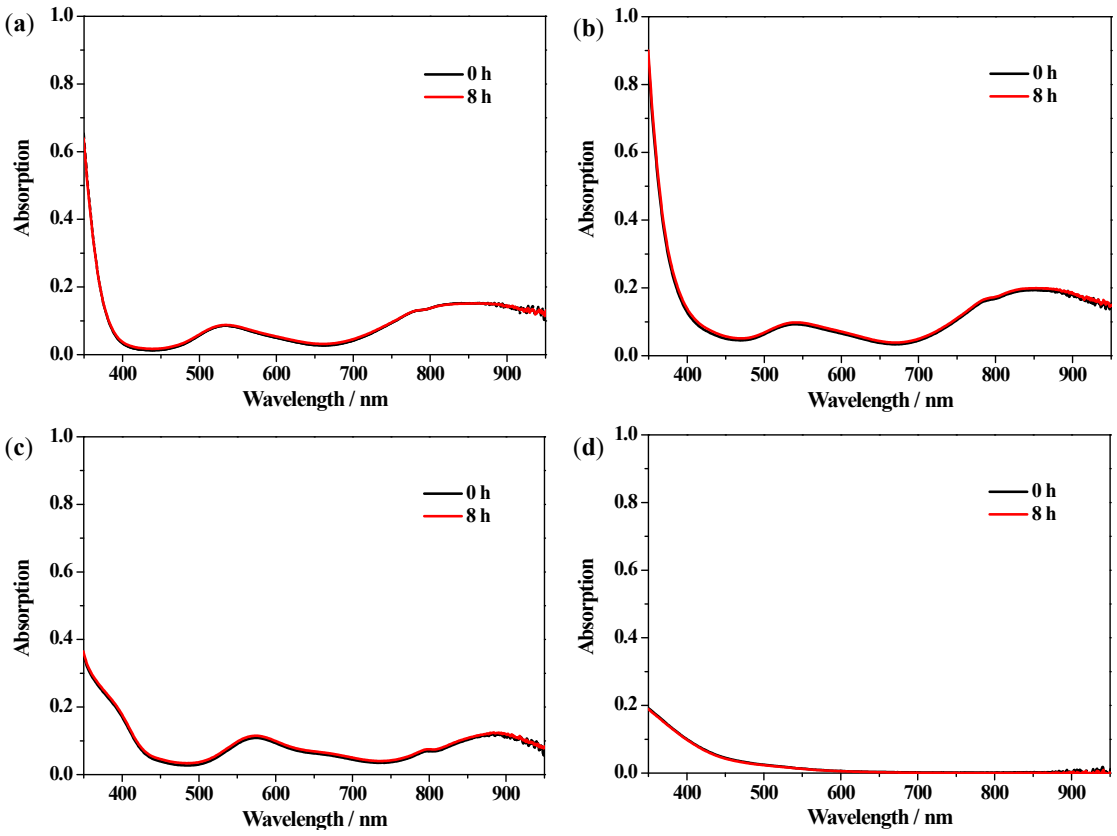

Fig. S4 Time-dependent UV-vis absorption spectra of 10 mM complexes **1** (a), **2** (b), **3** (c) and **5** (d) in 0.1 M PBS at pH 9.0.

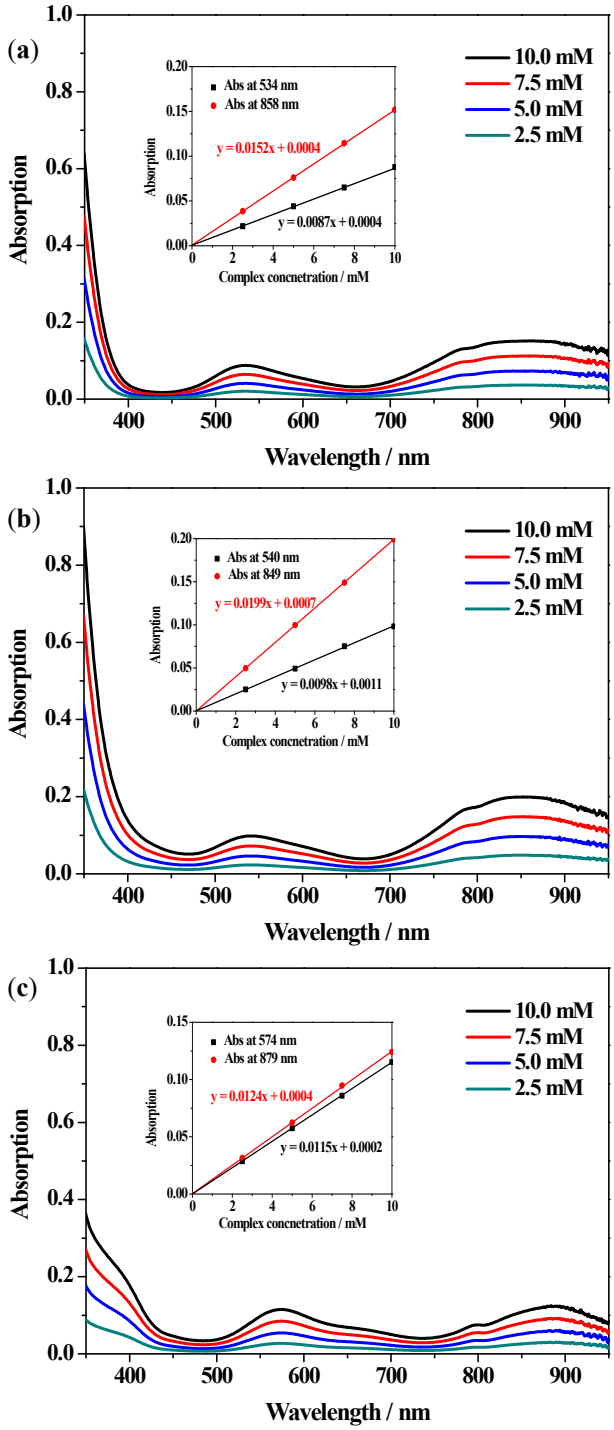

Fig. S5 The Concentration-dependent UV-vis absorption of complexes **1** (a), **2** (b) and **3** (c).

Table S5 The UV-vis absorption properties of complexes **1**–**3** and **5**

Complex	λ_1 / nm	ε_1 / M^{-1} cm^{-1}	λ_2 / nm	ε_2 / M^{-1} cm^{-1}
1	534	8.7	858	15.2
2	540	9.8	849	19.9
3	574	11.5	879	12.4

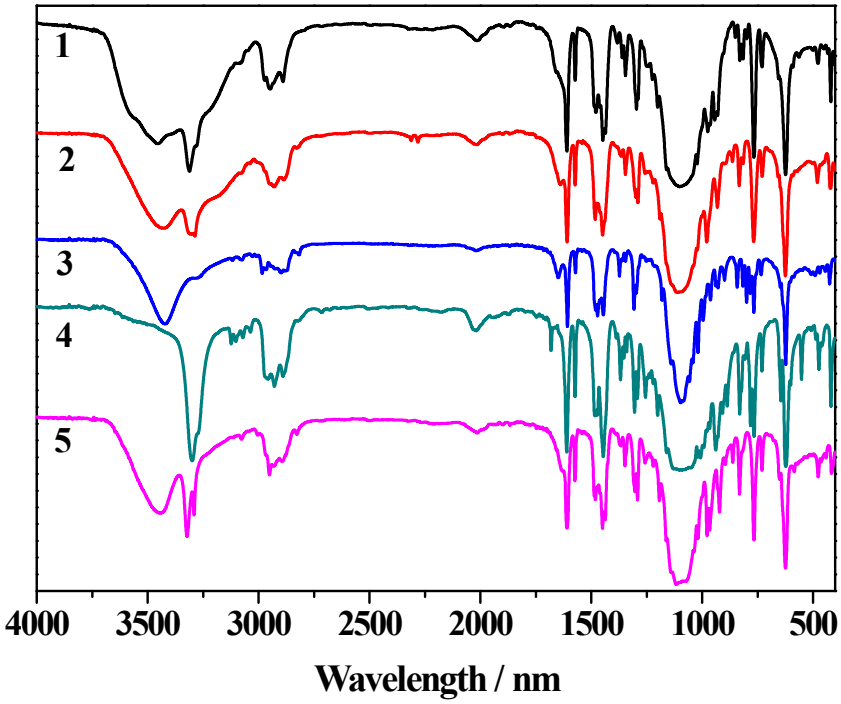

Fig. S6 Infrared spectrum of complexes **1**–**5**.

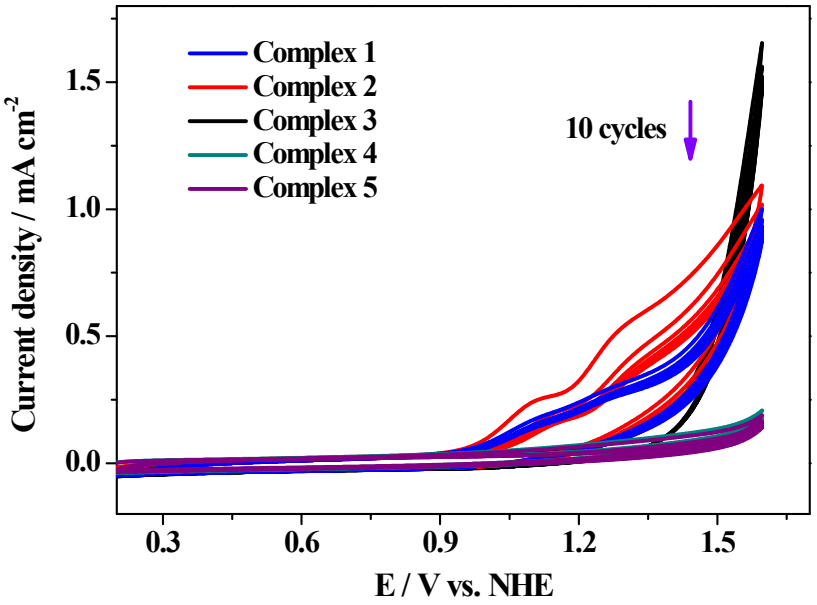

Fig. S7 Consecutive CV cyclic scan curves of 1 mM of complexes **1**–**5** in phosphate buffer solution (PBS) at pH 9.0, scan rate = 100 mV/s.

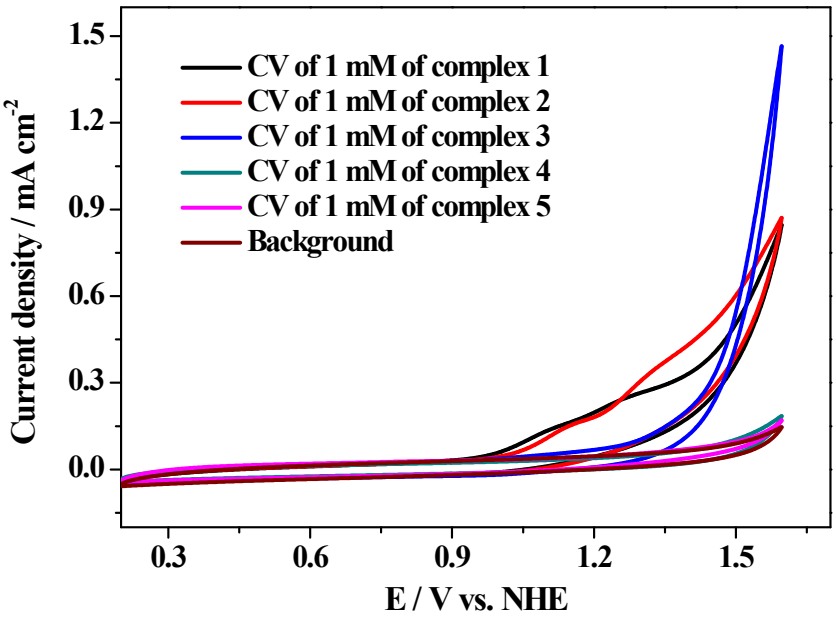

Fig. S8 CV scan curves of 1 mM of complexes **1**–**5** in PBS at pH 9.0, scan rate = 100 mV/s.

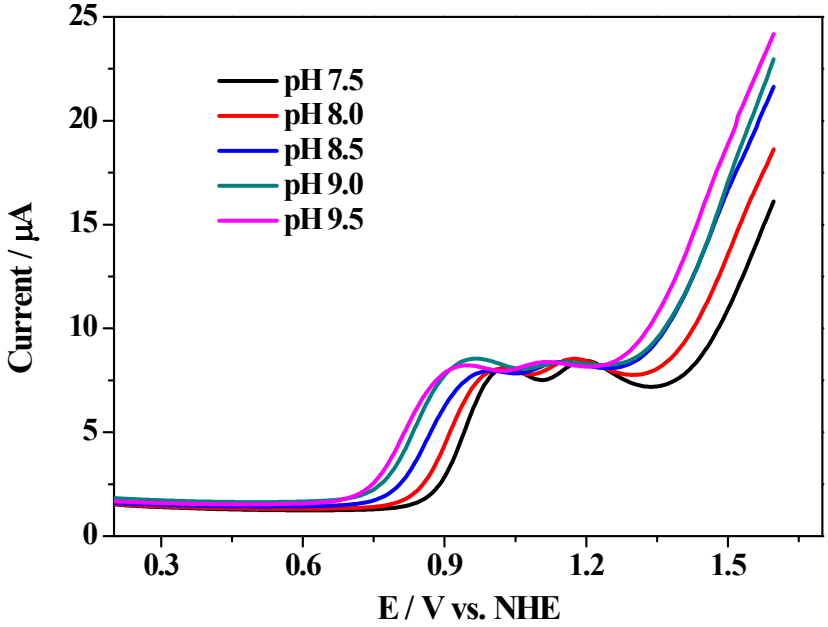

Fig. S9 DPV tests of 1.0 mM of complex **1** in 0.1 M PBS at various pH.

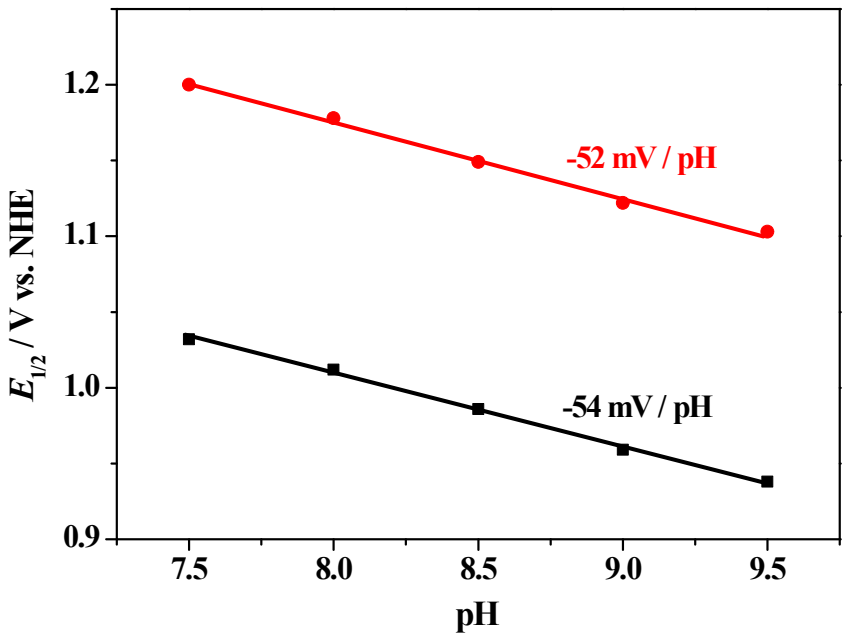

Fig. S10 Pourbaix diagram of complex **1** in 0.1 M PBS pH range of 7.5–9.5.

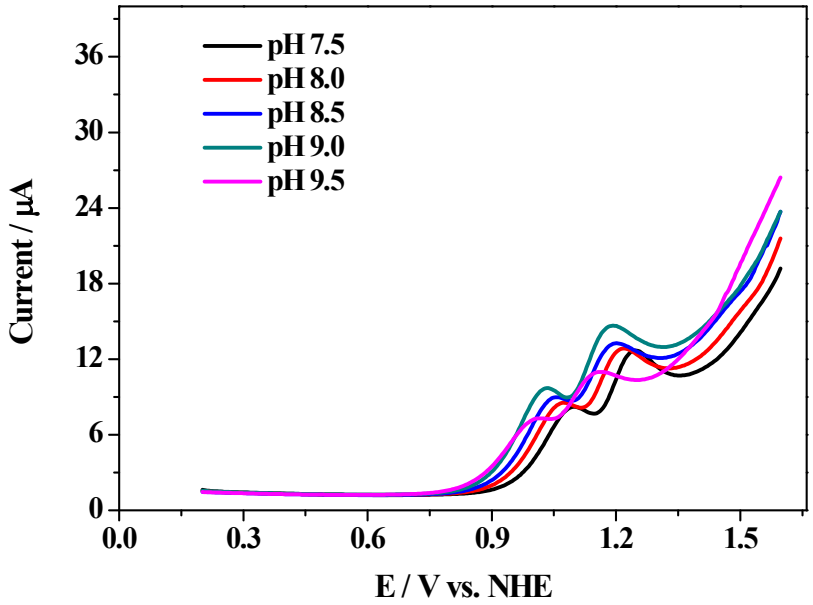

Fig. S11 DPV tests of 1.0 mM of complex **2** in 0.1 M PBS at various pH.

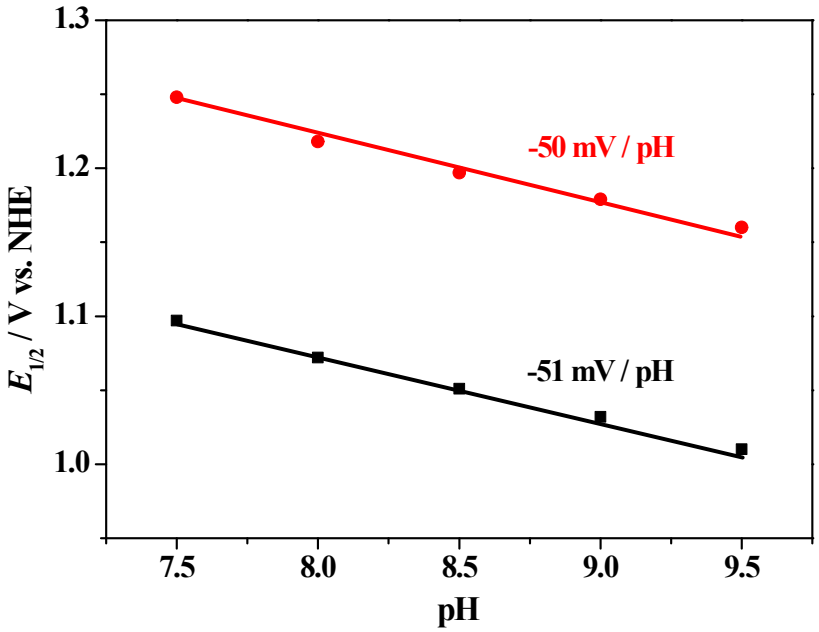

Fig. S12 Pourbaix diagram of complex **2** in 0.1 M PBS pH range of 7.5–9.5.

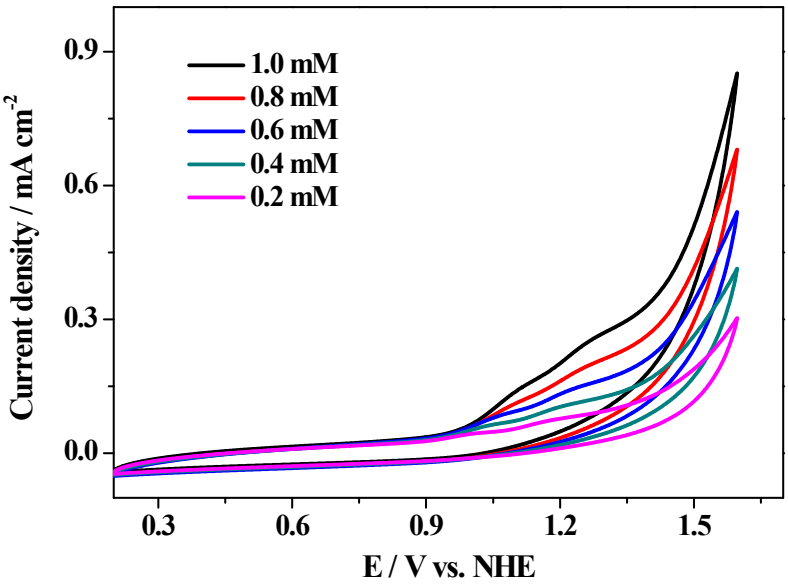

Fig. S13 CV of complex **1** with various concentrations in 0.1 M PBS at pH 9.0, scan rate = 100 mV/s.

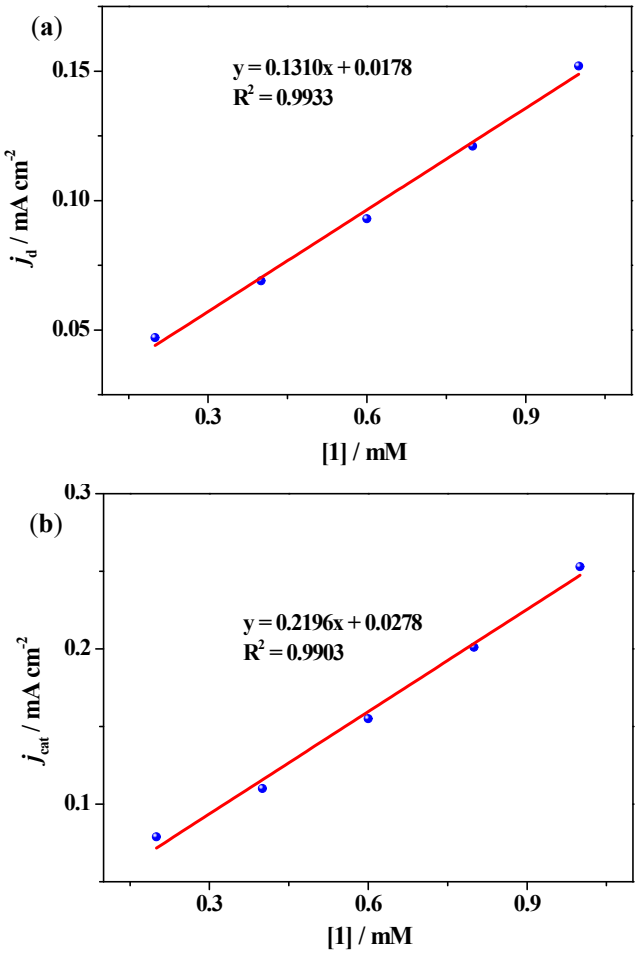

Fig. S14 Plots of the ratio of j_d (a) and j_{cat} (b) versus the concentration of complex **1**, scan rate = 100 mV/s.

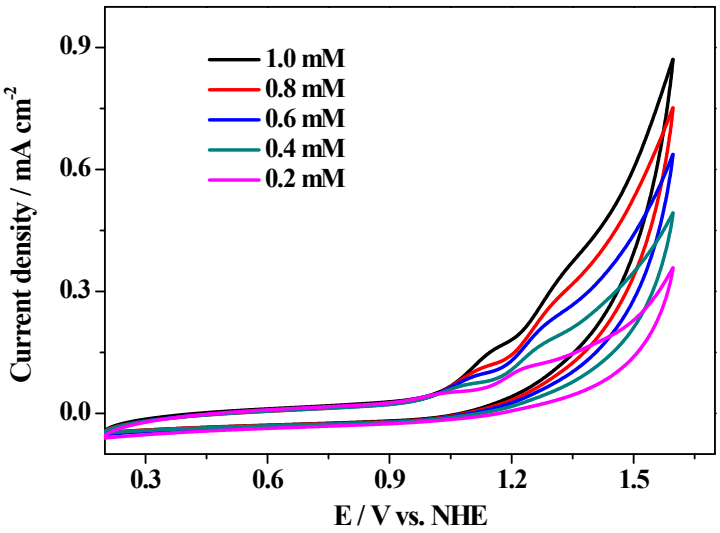

Fig. S15 CV of complex **2** with various concentrations in 0.1 M PBS at pH 9.0, scan rate = 100 mV/s.

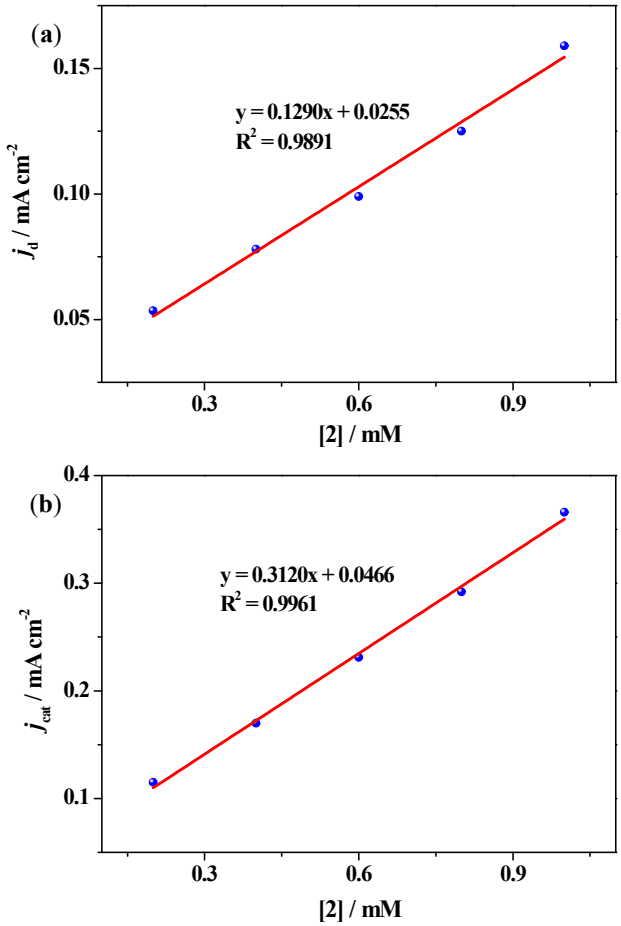

Fig. S16 Plots of the ratio of j_d (a) and j_{cat} (b) versus the concentration of complex **2**, scan rate = 100 mV/s.

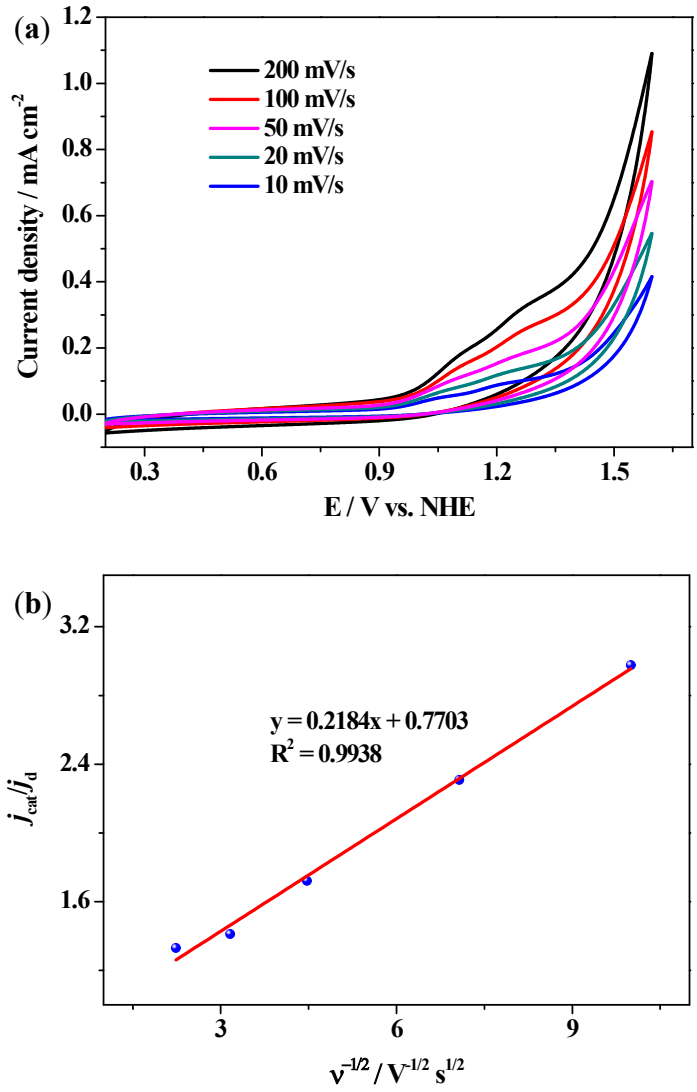

Fig. S17 CV of 1.0 mM of **1** in 0.1 M PBS at pH 9.0 with scan rate varying from 10 to 100 mV s^{-1} (a) and plots of the ratio of j_{cat} to j_d of **1** versus the reciprocal of the square root of the scan rate (b).

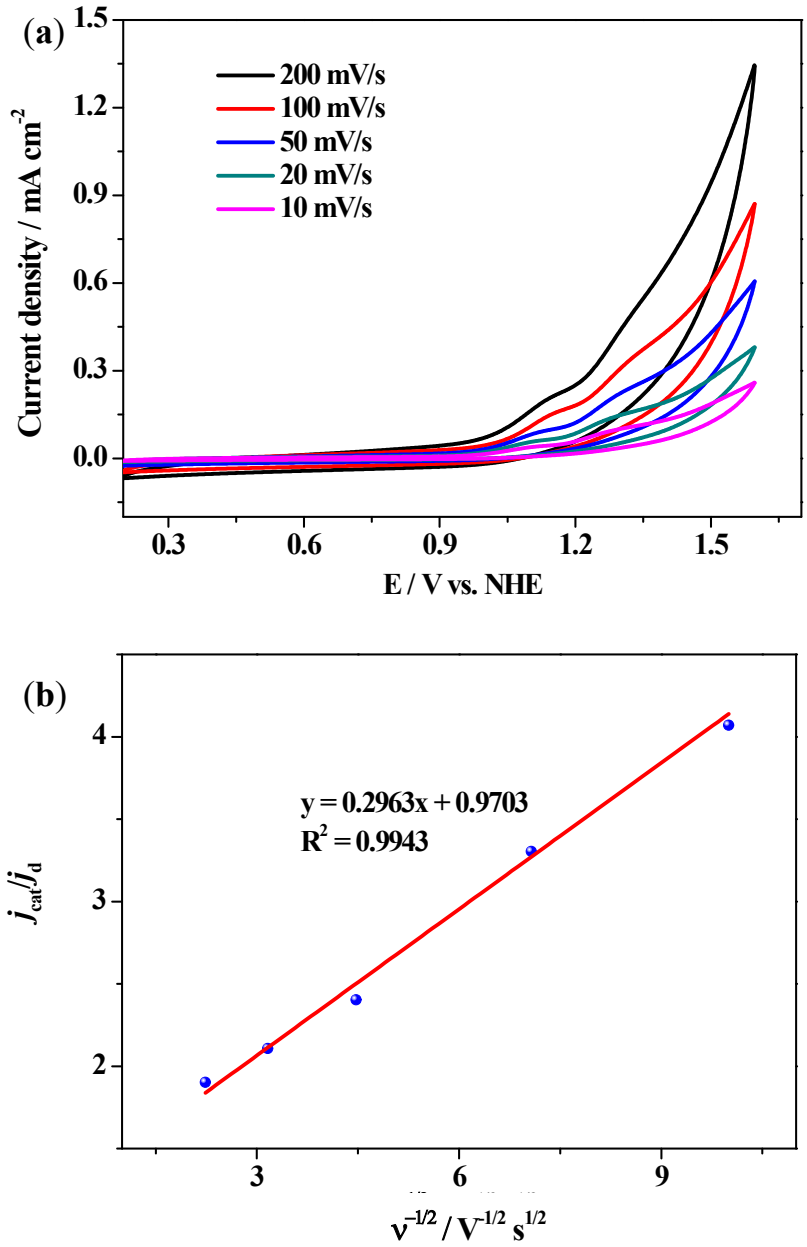

Fig. S18 CV of 1.0 mM of **2** in 0.1 M PBS at pH 9.0 with scan rate varying from 10 to 100 mV s^{-1} (a) and plots of the ratio of j_{cat} to j_d of **2** versus the reciprocal of the square root of the scan rate (b).

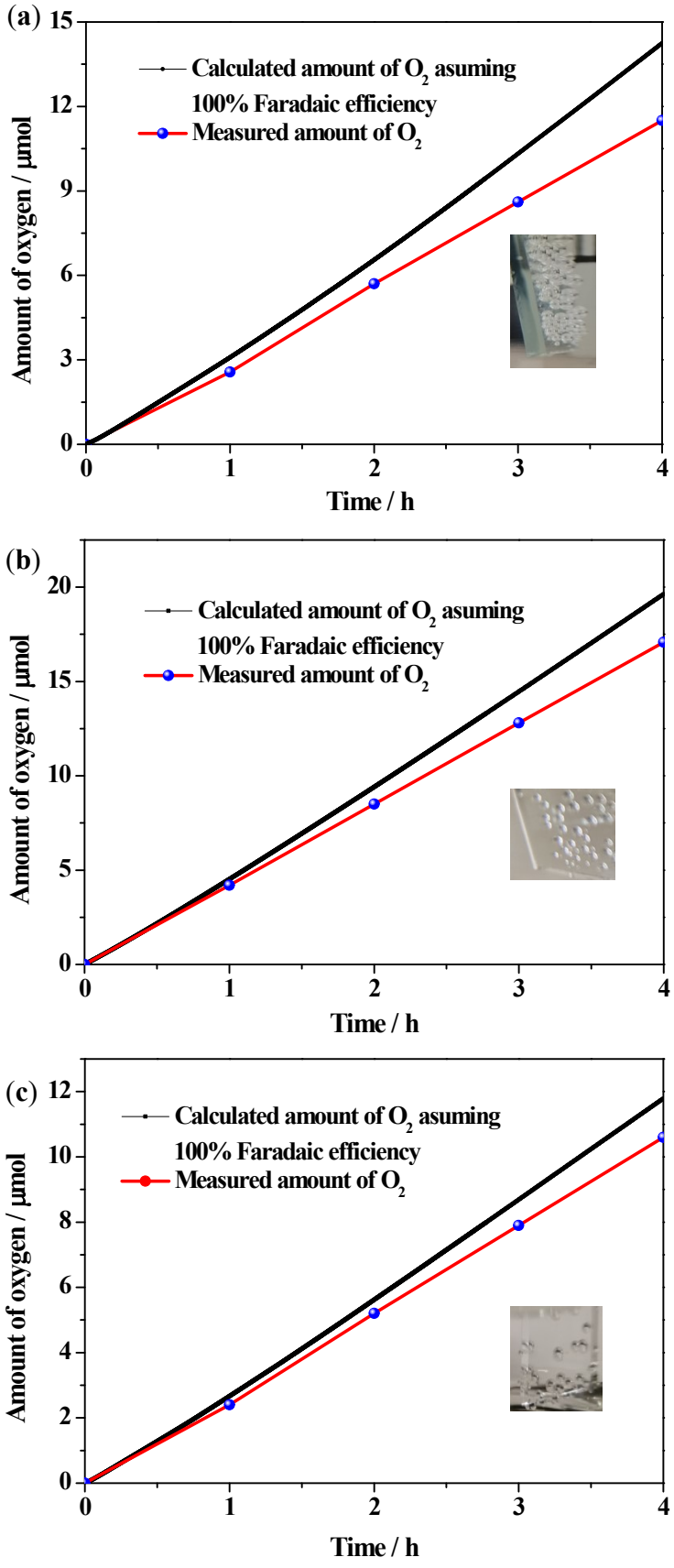

Fig. S19 Faradaic efficiency of O_2 evolution for **1** (a), **2** (b), and **3** (c) under 4 h of electrolysis at 1.45 V vs. NHE in 0.1 M PBS at pH 9.0.

Table S6 The electrocatalytic date toward water oxidation mediated by three nickel complexes

Complex	TOF / s^{-1}	Potential of j = 0.5 mA cm^{-2} / V	j at 1.45 V / mA cm^{-2}
1	0.014	1.50	0.40
2	0.027	1.45	0.52
3		1.44	0.32

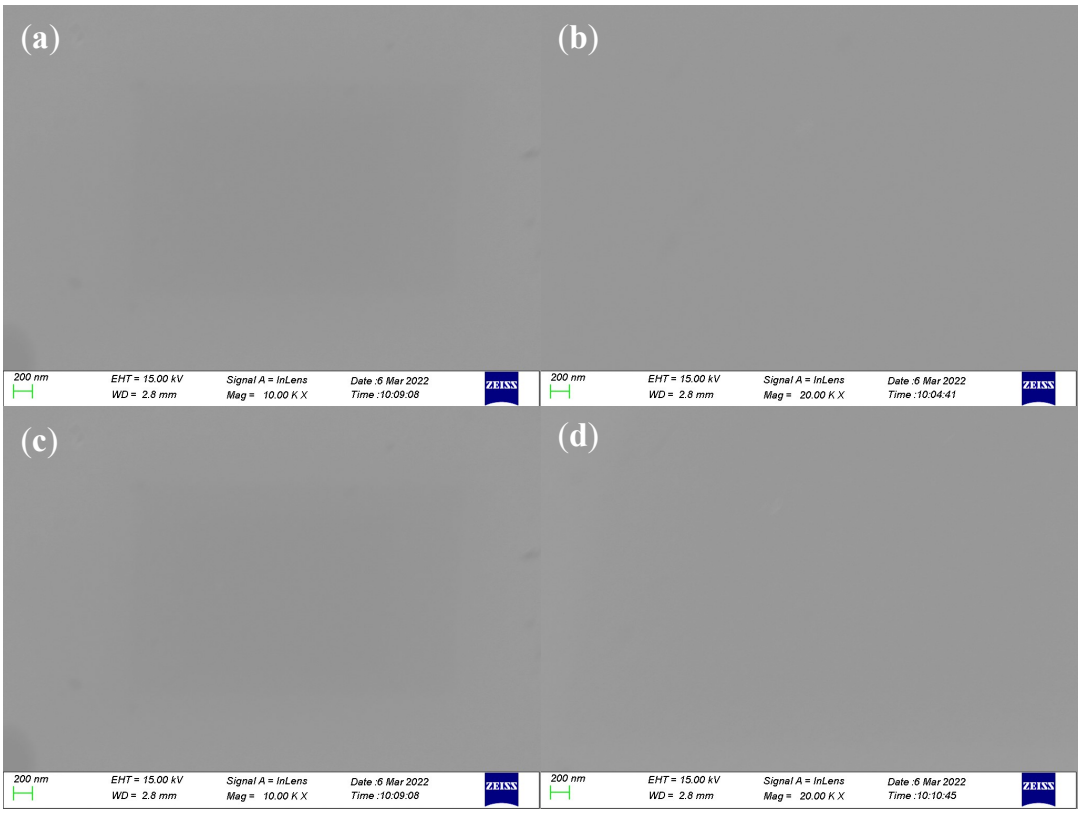

Fig. S20 SEM images of the surface of ITO electrode before (a) and after 4 h CPE experiments of 1 mM of **1** (b), **2** (c) and **3** (d) in 0.1 M PBS at pH = 9.0.

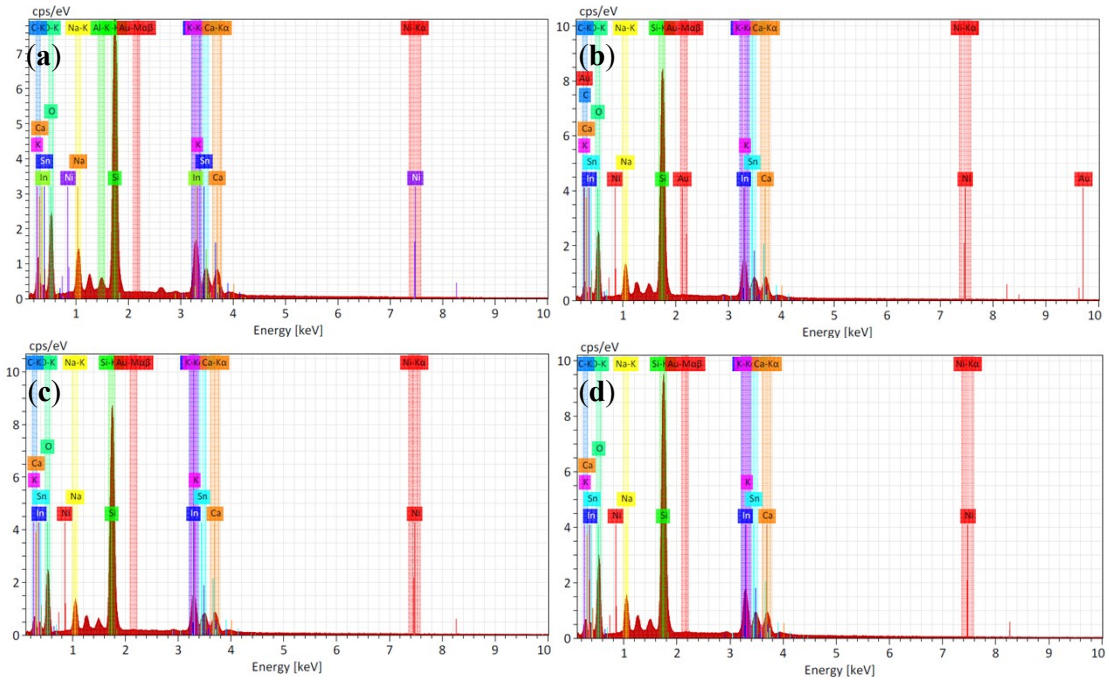

Fig. S21 EDX analysis result of the surface of ITO electrode before (a) and after 4 h CPE experiments of 1 mM of **1** (b), **2** (c) and **3** (d) in 0.1 M PBS at pH = 9.0.

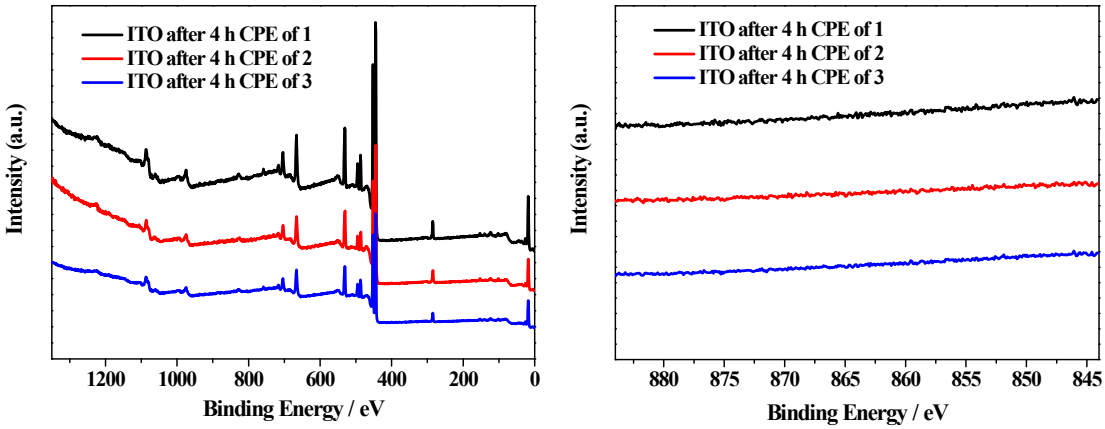

Fig. S22 Full XPS spectra (left) and XPS spectra of Ni element (right) on ITO electrode used for 4 h CPE test of complexes **1**–**3** at 1.45 V vs. NHE with 0.1 M PBS at pH 9.0 as electrolyte.